INTERNATIONAL JOURNAL FOR NUMERICAL METHODS IN FLUIDS
Int. J. Numer. Meth. Fluids 2002; **40**:457–465 (DOI: 10.1002/fld.299)

Integral boundary conditions for unsteady biomedical CFD applications

F. Nicoud*,† and T. Schönfeld

CERFACS, 42 Av. Gaspard Coriolis, 31057 Toulouse, France

SUMMARY

A methodology to prescribe integral boundary conditions is proposed. The approach makes use of the decomposition of the solution into waves. It applies to any numerical method solving hyperbolic equations, including the compressible Navier–Stokes equations or their incompressible counterpart when solved through an artificial compressibility method. For any physical quantity to be imposed (e.g. the mass flow rate entering the computational domain), the boundary treatment consists in imposing a 1D incoming 'acoustic' wave proportional to the difference between the mean quantity of interest (e.g. the mean mass flow rate) over the boundary and its prescribed target value. The approach is validated by computing both steady and pulsated channel flows for Womersley number upto 15. Results from a 3D simulation of the blood flow within a human aortic arch are briefly discussed. Copyright © 2002 John Wiley & Sons, Ltd.

KEY WORDS: computational fluid dynamics; biomechanics; blood flow; boundary conditions

1. INTRODUCTION AND MOTIVATION

Vascular diseases such as atherosclerosis and aneurysms are becoming frequent disorders in the industrialized world due to sedentary way of life and rich food. Causing more deaths than cancer, cardiovascular diseases are the leading cause of death in the western world. In recent years, encouraging advances in diagnostics have been made thanks to progress in medical imaging, including the following modalities: computed tomography (CT), magnetic resonance (MRI), ultrasound (US). However, the current exploitation of these new powerful imaging modalities remains mostly qualitative. An improved quantitative knowledge and understanding of the hemodynamic conditions in the treated region would be helpful to address and to solve certain basic problems related to therapy techniques (e.g. the re-stenosis in arteries treated by angioplasty). Measuring detailed blood flow features *in vivo* is obviously very challenging, although some recent progress in Doppler analysis have been performed.

*Correspondence to: F. Nicoud, Université Montpellier II, Department of Mathematics, CC051, 34095 Montpellier Cedex 5, France.
†E-mail: nicoud@math.univ-montp2.fr

Copyright © 2002 John Wiley & Sons, Ltd.
Received May 2001
Revised September 2001

In recent years, computational fluid dynamics (CFD) techniques have been used increasingly by researchers seeking to understand vascular hemodynamics. Most of the CFD-based hemodynamic studies so far have been conducted to represent *in vitro* conditions within restrictive assumptions. Perktold *et al.* [1] used a finite element based method to compute the pulsatile flow of a Newtonian fluid in a model of a carotid artery bifurcation. This work gave access to a detailed representation of the velocity, pressure and wall shear stress fields within the rigid walled approximation and the effect of the bifurcation angle on hemodynamic conditions was examined as well (see Reference [2] for the application of CFD methods to the design of end-to-side anastomoses). In an investigation of the effect of wall compliance on pulsatile flow in the carotid artery bifurcation, Perktold and Rappitsch [3] describe a weakly coupled fluid–structure interaction finite element method for solving fluid flows and vessel mechanics. The fluid–structure interaction problem was also investigated from a more mathematical point of view by Formaggia *et al.* [4] and in a 2D end-to-side anastomosis by Steinman *et al.* [5]. Rappitsch and Perktold [6] describe the transport of albumin in a model of a stenosis while Kunov *et al.* [7] propose a methodology to compute particle residence time in vessels. These studies under *in vitro* conditions are well suited to investigate basic phenomena related to fluid dynamics in vessels models but are not fully representative of actual patient hemodynamic conditions.

CFD methods possess also the potential to augment the data obtained from *in vivo* methods by providing a complete characterization of hemodynamic conditions (blood velocity and pressure as a function of space and time) under precisely controlled conditions. Milner *et al.* [8] used MRI data of two normal subjects to provide the boundary conditions (i.e. geometry and flow rates) for a CFD simulation of the blood flow patterns. This study showed that conventional 'averaged' carotid bifurcation models mask interesting hemodynamic features observed in realistic models derived from non invasive imaging of normal human subjects. Moreover, observation of inter-subject variations in the *in vivo* wall shear stress patterns supports the notion that more conclusive evidence regarding the role of hemodynamics in vascular disease may be derived from such individual studies.

Specific difficulties in CFD studies of blood flows are related to the boundary conditions. First of all, it is now recognized that the blood flow in a given district may depend on the global dynamics of the whole circulation. Consequently, it is sometimes necessary to couple the 3D blood flow solver to a low order model for the entire vascular system [9]. A second difficulty is related to the limitations of the existing *in vivo* anemometry techniques. Indeed, the space resolution is far too coarse to tackle even the largest scales of the blood flow details. As a consequence, the boundary conditions (e.g. the instantaneous velocity profile at the inlet section of the computed domain) are unknown for an *in vivo* blood flow computation. Most of the times, one assumes some analytical space–time evolution for prescribing the inlet profile. Taylor *et al.* [10] propose to assume very long circular vessel geometry upstream the inlet section so that the analytical solution of Womersley [11] can be prescribed. However, it is not always justified to assume a circular cross-section. An alternative approach based on a characteristic boundary treatment is proposed in this paper.

The characteristic method for prescribing boundary conditions is recalled in Section 2.1 and the modification proposed is detailed in Section 2.2. A simple validation test case is discussed in Section 2.3. Finally, we have used CT images of a pathological aortic arch together with Doppler velocity measurements to compute the blood flow in pulsatile conditions (Section 3). Concluding remarks are given in Section 4.

Copyright © 2002 John Wiley & Sons, Ltd.

2. BOUNDARY CONDITIONS

The characteristic Mach number in blood flows is obviously close to zero and for this study it would be more efficient to solve the incompressible Navier–Stokes equations. However, a compressible 3D solver [12] has been used for two reasons: (1) using a compressible flow solver allows us to propose a boundary treatment usable for applications where compressibility plays a major role (e.g. thermo-acoustic instabilities) and where the lack of accurate spatially resolved data (as discussed above) is also an issue; (2) certain efficient numerical techniques (e.g. artificial compressibility) to solve the incompressible Navier–Stokes equations lead to an hyperbolic problem. Thus they share a common mathematical behavior with the compressible equations; noticeably they allow the use of characteristic based boundary conditions.

2.1. Characteristic treatment

Characteristic treatment of boundary conditions for the Euler equations relies on determining the strength of the waves entering the computational domain as a function of the strength of the outgoing waves and the physical boundary conditions.

The 2D Euler equations may be expressed in quasi-linear form as

$$\frac{\partial \mathbf{V}}{\partial t} + \mathbf{A}\frac{\partial \mathbf{V}}{\partial x} + \mathbf{B}\frac{\partial \mathbf{V}}{\partial y} = 0 \tag{1}$$

Here $\mathbf{V} = (\rho, u, v, P)^{\mathrm{T}}$ is the vector of primitive variables and each of the Jacobian matrices $\mathbf{A}$ and $\mathbf{B}$ has its own complete set of real eigenvalues and right and left-eigenvectors. The matrix $\mathbf{E}_n$ defined as $\mathbf{A}n_x + \mathbf{B}n_y$ can be introduced, where $\vec{n}$ is chosen as the outward normal to the boundary under consideration. By diagonalizing $\mathbf{E}_n$ the eigenvalue matrix

$$\Lambda_n = \mathbf{L}_n \mathbf{E}_n \mathbf{L}_n^{-1} = \mathrm{diag}(\lambda_n^1, \lambda_n^2, \lambda_n^3, \lambda_n^4) = \mathrm{diag}(u_n, u_n, u_{n+c}, u_n - c) \tag{2}$$

is obtained where $u_n = \vec{u}.\vec{n}$ and c is the speed of sound. The matrices $\mathbf{L}_n$ ($\mathbf{L}_n^{-1}$) with left (right) eigenvectors as rows (columns) relate variations in the characteristic variables $\mathbf{W}_n$ to variations in the primitive vector $\mathbf{V}$ through the relations

$$\delta \mathbf{W}_n = \mathbf{L}_n \delta \mathbf{V}, \quad \delta \mathbf{V} = \mathbf{L}_n^{-1} \delta \mathbf{W}_n \tag{3}$$

Applying an explicit Euler time discretization to Equation (1), the update of primitive variables can be written as

$$\Delta \mathbf{V} = \mathbf{V}^{n+1} - \mathbf{V}^n = -\Delta t \mathscr{R} = -\Delta t \left[\mathbf{A}\frac{\partial \mathbf{V}}{\partial x} + \mathbf{B}\frac{\partial \mathbf{V}}{\partial y} \right] \tag{4}$$

For a given boundary with normal $\vec{n}$, the full residual $\mathscr{R}$ of Equation (4) can be split into a *normal* component $\mathscr{R}_n$ (involving only normal derivatives) and a *tangential* component $\mathscr{R}_s$ (involving only derivatives along $\vec{s}$, where $\vec{s}$ forms an orthonormal basis $(\vec{n}, \vec{s})$ with $\vec{n}$). Let us define $\mathbf{V}^n$ as the boundary value at time level n, and $\delta \mathbf{V}^{\mathrm{P}}$ the predicted boundary update from the interior scheme, prior to application of the boundary condition. Although it is not the only possible choice [13], we will assume in the remainder of this paper that the boundary condition is applied to the *normal* update i.e. $\delta \mathbf{V}_n^{\mathrm{P}} = -\Delta t \mathscr{R}_n$. It follows that $\delta \mathbf{V}^U = \delta \mathbf{V}^{\mathrm{P}} - \delta \mathbf{V}_n^{\mathrm{P}}$ (which would also contain the viscous terms if the Navier–Stokes equations are considered) is not

Copyright © 2002 John Wiley & Sons, Ltd.

affected by the boundary condition. Consistently, the amplitude of the characteristic waves will be calculated as $\mathscr{A}_i = \lambda_i \partial W_n^i / \partial n$ (no summation). Typically, the characteristic based boundary treatment is applied as follows:

1. From Equation (3), decompose $\delta \mathbf{V}_n^{\mathrm{P}}$, into characteristic variations $\delta W_n^{\mathrm{in,P}}$ and $\delta W_n^{\mathrm{out}}$ due to in-going and outgoing waves, with corresponding primitive variations $\delta \mathbf{V}_n^{\mathrm{in,P}}$ and $\delta \mathbf{V}_n^{\mathrm{out}}$.
2. Modify the amplitude of the incoming wave(s) $\delta W_n^{\mathrm{in,P}}$ according to the physical requirements at the boundary. This produces the corrected amplitudes, $\delta W_n^{\mathrm{in,C}}$. Retain the outgoing waves $\delta W_n^{\mathrm{out}}$ or $\delta \mathbf{V}_n^{\mathrm{out}}$ as they are.
3. Combine the waves $\delta W_n^{\mathrm{in,C}}$ and $\delta W_n^{\mathrm{out}}$, and using $\mathbf{L}_n^{-1}$, Equation (3), transform back to primitive variables. This gives $\delta \mathbf{V}_n^{\mathrm{C}}$. The boundary point is then updated as

$$\mathbf{V}^{n+1} = \mathbf{V}^n + \delta \mathbf{V}^U + \delta \mathbf{V}_n^{\mathrm{C}} = \mathbf{V}^n + \delta \mathbf{V}^U + \delta \mathbf{V}^{\mathrm{in,C}} + \delta \mathbf{V}^{\mathrm{out}}$$

2.2. *Approximate boundary conditions*

The classical characteristic formulation is widely used since it provides a theoretical basis to derive proper boundary condition treatments, following steps 1 and 3 above. For example, in the case of a given inlet velocity profile imposed, say $u_n = u_{\mathrm{ref}}$, it results from the formalism in Section 2.1 that the in-going acoustic wave is related to the outgoing one as follows [14]:

$$\mathscr{A}_4 = \mathscr{A}_3 + 2 \frac{\mathrm{d}u_{\mathrm{ref}}}{\mathrm{d}t} \tag{5}$$

It follows that the boundary condition is fully reflecting acoustically: any physical or numerical perturbation generated during the calculation cannot leave the computational domain. To ensure the stability of the simulation, one often makes use of dissipative schemes in order to damp the perturbations that cannot be evacuated through the boundaries. However, using dissipative numerical schemes for calculating unsteady flows, e.g. the blood flow in arteries, may lead to erroneous results [15]. Experience proves that it may be sufficient, and safer numerically, to prescribe the normal velocity approximately by imposing the in-going wave as

$$\mathscr{A}_4 = K_u (u_n - u_{\mathrm{ref}}) \tag{6}$$

where K_u is a relaxation coefficient. This is similar to what proposed Rudy and Strikwerda [16] to overcome the lack of pressure reference when fully non-reflecting outlet conditions are used. They showed that the relaxation coefficient is related to the characteristic size of the domain and the characteristic Mach number. Condition (6) is virtually non-reflecting if u_n is close to u_{ref} but prevents u_n from being too different from the reference. Note that, contrary to the full reflecting formulation (5), Equation (6) does not guaranty that u_n is strictly equal to u_{ref}. Note however that the reference velocity is not known precisely in practical blood flow simulations. Both formulations (5) and (6) require the knowledge of u_{ref} *pointwise* at the boundary. However, this information is never available due to *in vivo* anemometry limitations; the access to the bulk velocity $u_{\mathrm{ref,bulk}}$ is easier. The simple approximate integral condition that we propose then becomes, integrating the RHS of Equation (6) over the boundary B:

$$\mathscr{A}_4 = K_u \left(\frac{1}{S_B} \int_B u_n \, \mathrm{d}S_B - u_{\mathrm{ref,bulk}} \right) \tag{7}$$

Copyright © 2002 John Wiley & Sons, Ltd.

where S_B is the area of B. In this formulation, the incoming acoustic wave depends only on *time* and drives the total flow rate entering the domain through B. The shape of the velocity profile comes out from the terms not modified by the boundary treatment, i.e. $\delta\mathbf{V}^U$ in Section 2.1. Note that the integral term in (7) is assessed at each iteration of the simulation and the input $u_{\text{ref, bulk}}$ is a function of time only. Similar relation can easily be provided in order to control the bulk velocity at a subsonic outlet boundary.

2.3. Pulsatile Poiseuille flow

In order to validate this approximate integral boundary condition, an unsteady Poiseuille flow computation has been carried out. The averaged bulk Reynolds number is $Re_h = 870$ with h half the channel cross-section. The length of the straight channel is $40h$. The unsteady flow is pulsated at frequencies defined by the Womersley number $Wo = h\sqrt{\omega/\nu} = 15$ (this value is characteristic for blood flows in large arteries) with ω the pulsation of the flow rate variation. The maximal amplitude is 45% of the mean flow rate. At the channel inlet the integral values of both the flow rate and the temperature are imposed, while at the outlet only the integral value of the flow rate is imposed.

Figure 1 shows the velocity profiles at the inlet at outlet sections at three different instances. The velocities are scaled by the mean flow velocity $\langle U_{\text{bulk}} \rangle$. The CFD results are compared to the analytical solution [11] obtained by assuming no dependence in the streamwise direction in a channel submitted to a pressure gradient of the form $\nabla P = \nabla P_0 + \nabla P_1 \exp(\mathrm{j}\omega t)$, that is

$$u(y,t) = -\frac{\nabla P_0}{2\mu}(h^2 - y^2) + \Re\left[\mathrm{j}\frac{\nabla P_1}{\rho\omega}\left(1 - \frac{\cos(\alpha y/h)}{\cos(\alpha)}\right)\right]$$

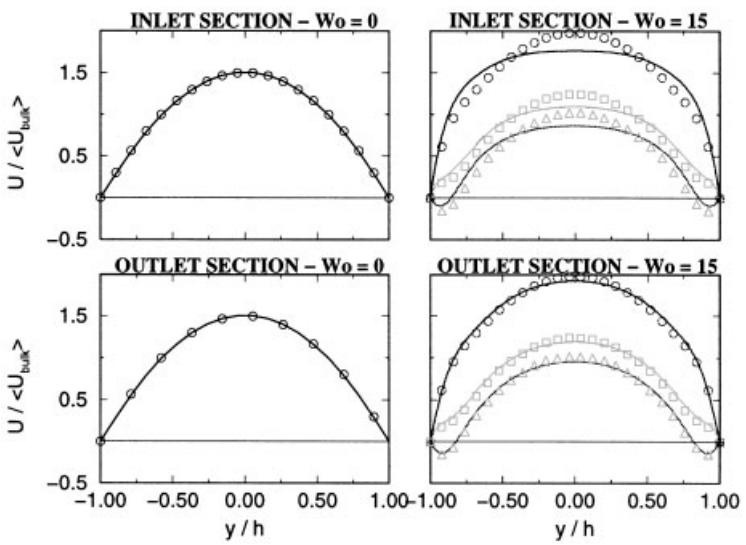

Figure 1. Velocity profiles for steady (left column) and unsteady (right column) Poiseuille flow, at inlet (top row) and outlet (bottom row). Lines indicate CFD calculations, symbols correspond to the analytical solution. Three different phases (0, 70 and 180°) are shown for the case $Wo = 15$.

Copyright © 2002 John Wiley & Sons, Ltd.

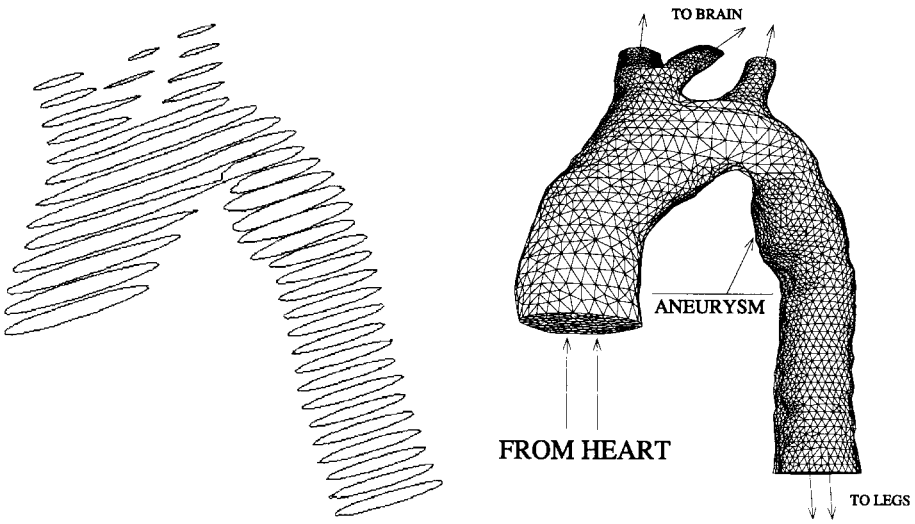

Figure 2. Contours obtained from the segmentation process (left) and surface grid of aorta (right).

where y is the normal co-ordinate, μ is the dynamic viscosity, ρ is the fluid density, $\nu = \mu/\rho$ and $\alpha = Wo\exp(3j\pi/4)$ is proportional to the Womersley number.

Figure 2 reveals a good agreement along the cross-section. It appears that the application of sucking outlet conditions is simpler to realize than imposing 'blowing' inlet conditions. This is because the time scale of the diffusion terms in the normal (to the wall) direction is larger than the time scale of the unsteadiness (the Womersley number is a measure of the ratio between these two characteristic times). For smaller values of Wo, this is no longer the case and the results at the inlet improve. In the limit $Wo \to 0$, the integral boundary treatment allows to recover exactly the parabolic (Poiseuille) profile.

3. BIO-MEDICAL FLOW SIMULATIONS

From a set of CT images of a human thorax, a level set method (e.g. Reference [17]) has been used plane by plane in order to identify and digitalize the position of the aorta lining. The output of this segmentation process is a stack of contours as shown in the LHS of Figure 2. We then make use of a commercial CFD mesh generator [18] in order to reconstruct the full arterial morphology through a triangular surface mesh discretization (RHS of Figure 2). Finally, a three-dimensional volume grid based on tetrahedra is generated with approximately 12 000 grid points and 60 000 elements.

A flow simulation was conducted over a time-span of several cardiac cycles. The flow field is initialized through flow at rest. At the inlet of the simulated domain (which corresponds to the outlet of the heart) pulsating inlet conditions were imposed, that correspond to the velocity data provided from Doppler anemometry. The inlet mass flow rate per cycle is approximately 5 l/min with the time evolution over one cycle shown in Figure 3. At the three upper outlet sections (corresponding to the brachiocephalic trunk, the common carotid

Copyright © 2002 John Wiley & Sons, Ltd.

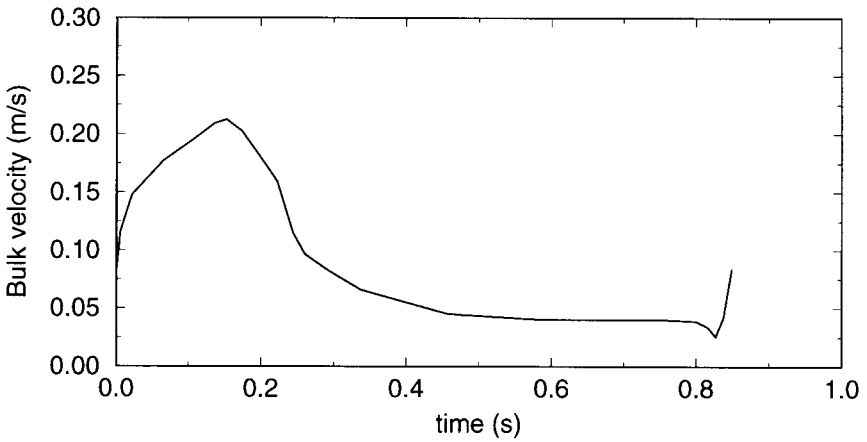

Figure 3. Time evolution of the inlet bulk velocity over one cycle. The area of the inlet section is close to 9 cm^2.

artery and the subclavian artery) the flow rate was prescribed as 15, 10 and 10% of the total flow rate respectively (using the integral boundary conditions described above). These are typical values for the corresponding bulk flow rates for a normal human subject. The remaining flow leaves the simulated domain through the descending outlet section. Here non-reflecting outflow conditions are applied.

A typical snapshot of the velocity normal to the inlet section is shown in the LHS of Figure 4. Thanks to the integral boundary condition, the shape of the velocity profile is smooth and consistent with the no slip condition on the edge of the cross-section. The profile is not symmetric because of the curvature in the ascending aorta (see Figure 2 right). Such a shape could not be reproduced by coupling the CFD solver with a low-order model or by prescribing the analytical solution of Womersley [11] (assuming very long circular vessel geometry upstream the inlet section). Note, however that, although plausible, the behaviour shown in Figure 4 (left) cannot be confirmed experimentally since no measurements are available. The visualization of the velocity vectors (RHS of Figure 4) indicates the emergence of an important recirculation zone in the upper section of the downstream section which is related to the aneurysm. Further investigations have shown that the particle residence time is increased by as much as 3 times because of this arterial disease and that the wall shear stress keeps a small value in the aneurysm area even during the systolic peak.

4. CONCLUDING REMARKS AND PERSPECTIVES

A new simple methodology to prescribe integral boundary conditions has been presented. In this approach, which makes use of the decomposition of the solution into waves, the incoming 'acoustic' wave is prescribed as proportional to the difference between the mean quantity of interest (e.g. the mean mass flow rate) over the boundary and its prescribed target value. The shape of the profile of the quantity prescribed at the boundary results from the

Copyright © 2002 John Wiley & Sons, Ltd.

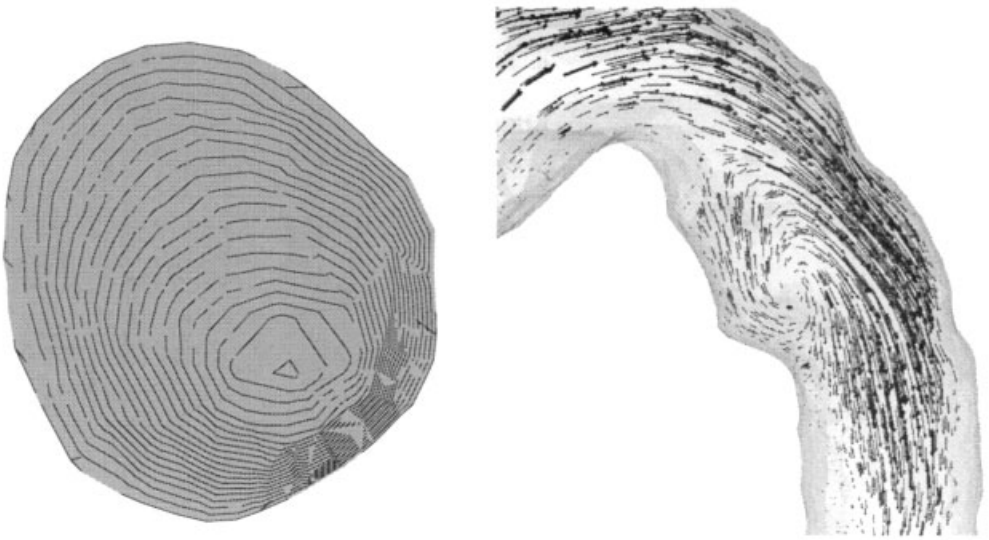

Figure 4. Iso-lines (increment is 0.025 m/s and the minimum value is zero) of the velocity normal to the inlet section (left) and velocity vectors indicating a recirculation zone near the aneurysm (right). Both views correspond to a time slightly after the systolic peak.

equilibrium between the different terms of the Navier–Stokes equations inside the computational domain. This integral type of boundary condition has been validated by computing the flow resulting from steady and unsteady pressure gradient in a channel. The numerical results are quantitatively in good agreement with the analytical solution for Womersley numbers up to 15.

From a numerical point of view, the integral approach decouples the ingoing and the outgoing waves and relaxes towards a non-reflecting condition when the relaxation coefficient tends to zero. For non-zero relaxation parameter, it is simple to show that this boundary condition acts as a low-pass filter in the sense that the reflexion coefficient is a decreasing function of the frequency. As a consequence, the high-frequency spurious perturbations possibly created within the computational domain are not reflected by this boundary condition and are filtered out. This makes the approximate boundary conditions discussed throughout this paper very different from the classical characteristic based treatment where the incoming waves are explicit functions of the outgoing ones. The net effect is that less artificial viscosity may be required to stabilize to calculation, a great advantage as far as unsteady CFD is concerned.

As an application, the flow in a human aortic arch has been computed. The geometry has been obtained from *in vivo* CT images and the unsteady bulk mass flow rate deduced from Doppler anemometry is used as a boundary condition. The integral boundary treatment presented in this paper provides a smooth plausible velocity profile at the inlet section of the computational domain. It is, however, difficult to assess precisely the benefit of the integral boundary treatment by considering this particular biomedical configuration since no measurements are available. At the moment, the only obvious advantage is that the only input required for such boundary treatment is a bulk information instead of a spatially resolved

Copyright © 2002 John Wiley & Sons, Ltd.

profile. Further, tests including *in vitro* configurations with more experimental details should be performed in the near future to establish the superiority of the integral approach. From a modeling point of view, the compliance of the wall as well as the non-Newtonian blood rheology should be accounted for in order to perform more realistic blood flow simulations in arteries.

ACKNOWLEDGEMENTS

The authors acknowledge Prof. H. Rousseau, Prof. G. Fournial and Dr. A. Elias, all members of the medical staff of CHU Rangueil in Toulouse, for providing scanner images and Doppler anemometry data. Most of the data extraction, geometry reconstruction and surface modeling tasks have been carried out by F. Cadene of CUST Clermont-Ferrand in the frame of his trainee stay at CERFACS.

REFERENCES

1. Perktold K, Resh M, Peter R. Three-dimensional numerical analysis of pulsatile flow and wall shear stress in the carotid artery bifurcation. *Journal of Biomechanics* 1991; **24**(6):409–420.
2. Lei M, Archie JP, Kleinstreuer C. Computational design of a bypass graft that minimizes wall shear stress gradients in the region of distal anastomosis. *Journal of Vascular Surgery* 1997; **25**:637–646.
3. Perktold K, Rappitsch G. Computer simulation of local blood flow and vessel mechanics in a compliant carotid artery bifurcation model. *Journal of Biomechanics* 1995; **28**(7):845–856.
4. Formaggia L, Gerbeau JF, Nobile F, Quarteroni A. On the coupling of 3D and 1D Navier–Stokes Equations for flow problems in compliant vessels. *INRIA—Research Report N. 3862*, 2000.
5. Steinman DA, Ethier CR. The effect of wall distensibility on flow in a two-dimensional end-to-side anastomosis. *Journal of Biomechanical Engineering* 1994; **116**:294–301.
6. Rappitsch G, Perktold K. Pulsatile albumin transport in large arteries: a numerical simulation study. *Journal of Biomechanical Engineering* 1996; **118**:511–518.
7. Kunov MJ, Steinman DA, Ethier CR. Particle volumetric residence time calculations in arterial geometries. *Journal of Biomechanical Engineering* 1996; **118**:158–164.
8. Milner JS, Moore JA, Steinman DA. Hemodynamics of human carotid artery bifurcations: computational studies with models reconstructed from magnetic resonance imaging of normal subjects. *Journal of Vascular Surgery* 1998; **28**:143–156.
9. Formaggia L, Nobile F, Quarteroni A, Veneziani A. Multiscale modelling of the circulatory system: a preliminary analysis. *Computing and Visualization in Science* 1999; **2**:75–83.
10. Taylor C, Hughes T, Zarins C. Finite element modeling of blood flow in arteries. *Computer Methods in Applied Mechanics and Engineering* 1998; **158**:155–196.
11. Womersley JR. Method for the calculation of velocity, rate of flow and viscous drag in arteries when the pressure gradient is known. *Journal of Physiology* 1955; **127**:553–563.
12. Schönfeld T, Rudgyard MA. Steady and unsteady flows simulations using the hybrid flow solver AVBP. *AIAA Journal* 1999; **37**(11):1378–1385.
13. Nicoud F. Defining wave amplitude in characteristic boundary conditions. *Journal of Computational Physics* 1999; **149**(2):418–422.
14. Poinsot TJ, Lele SK. Boundary conditions for direct simulations of compressible viscous flows. *Journal of Computational Physics* 1991; **101**:104–129.
15. Colin O, Rudgyard M. Development of high-order Taylor–Galerkin schemes for LES. *Journal of Computational Physics* 2000; **162**:338–371.
16. Rudy D, Strikwerda J. A nonreflecting outflow boundary condition for subsonic Navier–Stokes equations. *Journal of Computational Physics* 1980; **36**:55–70.
17. Malladi R, Sethian JA. Level set methods for curvature flow, image enhancement, and shape recovery in medical images. *Proceedings of Conference on Visualization and Mathematics*, Berlin, Germany, June, 1998.
18. CFDGEOM Tutorials. CFD Research Corporation, January 2000.

Copyright © 2002 John Wiley & Sons, Ltd.